

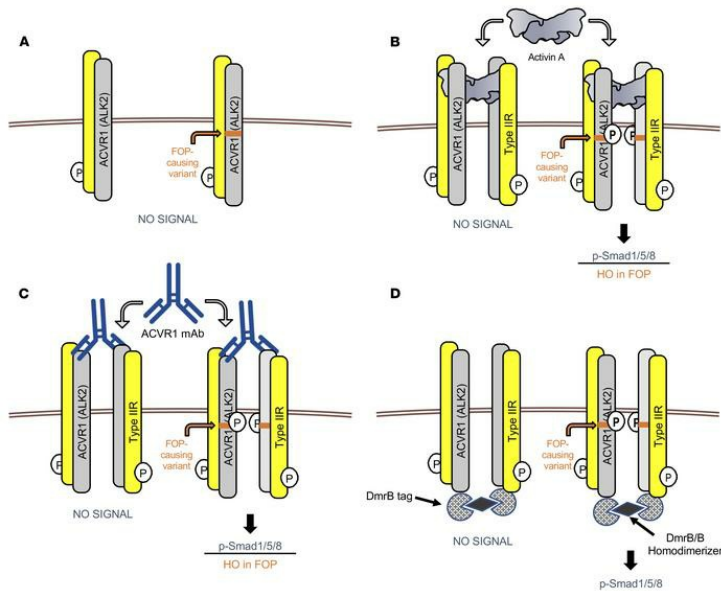
Anti-ACVR1 antibodies exacerbate heterotopic ossification in fibrodysplasia ossificans progressiva (FOP) by activating FOP-mutant ACVR1

Senem Aykul, ... , Vincent Idone, Sarah J. Hatsell

J Clin Invest. 2022;132(12):e153792. <https://doi.org/10.1172/JCI153792>.

Research Article Bone biology Therapeutics

Graphical abstract



Find the latest version:

<https://jci.me/153792/pdf>



Anti-ACVR1 antibodies exacerbate heterotopic ossification in fibrodysplasia ossificans progressiva (FOP) by activating FOP-mutant ACVR1

Senem Aykul,¹ Lily Huang,¹ Lili Wang,¹ Nanditha M. Das,¹ Sandra Reisman,¹ Yonaton Ray,¹ Qian Zhang,¹ Nyanza Rothman,¹ Kalyan C. Nannuru,¹ Vishal Kamat,¹ Susannah Brydges,¹ Luca Troncone,² Laura Johnsen,¹ Paul B. Yu,² Sergio Fazio,¹ John Lees-Shepard,¹ Kevin Schutz,³ Andrew J. Murphy,¹ Aris N. Economides,¹ Vincent Idone,¹ and Sarah J. Hatsell¹

¹Regeneron Pharmaceuticals Inc, Tarrytown, New York, USA. ²Department of Medicine, Cardiovascular Division, Brigham and Women's Hospital, Harvard Medical School, Boston, Massachusetts, USA.

³Adimab, Lebanon, New Hampshire, USA.

Fibrodysplasia ossificans progressiva (FOP) is a rare genetic disorder whose most debilitating pathology is progressive and cumulative heterotopic ossification (HO) of skeletal muscles, ligaments, tendons, and fascia. FOP is caused by mutations in the type I BMP receptor gene *ACVR1*, which enable *ACVR1* to utilize its natural antagonist, activin A, as an agonistic ligand. The physiological relevance of this property is underscored by the fact that HO in FOP is exquisitely dependent on activation of FOP-mutant *ACVR1* by activin A, an effect countered by inhibition of anti-activin A via monoclonal antibody treatment. Hence, we surmised that anti-*ACVR1* antibodies that block activation of *ACVR1* by ligands should also inhibit HO in FOP and provide an additional therapeutic option for this condition. Therefore, we generated anti-*ACVR1* monoclonal antibodies that block *ACVR1*'s activation by its ligands. Surprisingly, in vivo, these anti-*ACVR1* antibodies stimulated HO and activated signaling of FOP-mutant *ACVR1*. This property was restricted to FOP-mutant *ACVR1* and resulted from anti-*ACVR1* antibody-mediated dimerization of *ACVR1*. Conversely, wild-type *ACVR1* was inhibited by anti-*ACVR1* antibodies. These results uncover an additional property of FOP-mutant *ACVR1* and indicate that anti-*ACVR1* antibodies should not be considered as therapeutics for FOP.

Introduction

Fibrodysplasia ossificans progressiva (FOP) (OMIM #135100) is a rare, autosomal dominant disorder characterized by congenital skeletal dysplasias and progressive and cumulative heterotopic ossification (HO) of skeletal muscles, tendons, ligaments, and fascia (1). FOP arises from amino acid-altering mutations in the cytoplasmic domain of the type I bone morphogenetic protein (BMP) receptor activin A receptor type I (*ACVR1*), with the most

common mutation being c.617G>A, which changes arginine 206 to histidine (R206H) and occurs in approximately 95% of patients (2), but with multiple additional FOP-causing variants in the GS and kinase domains of *ACVR1* (3, 4).

This discovery sparked the question of what property these amino acid-altering mutations impart to *ACVR1*. Their location in the intracellular domain of this BMP receptor indicated that changes in ligand binding properties were unlikely, and therefore the focus was placed on the variants' signaling properties (2, 3). Initial investigations proposed that FOP-mutant *ACVR1* causes HO by being hyperactivated by BMP ligands or by displaying a certain level of constitutive activity (reviewed in refs. 5, 6). However, these investigations did not utilize genetically accurate in vivo models of FOP and did not query the physiological relevance of their findings.

Therefore, to investigate the molecular mechanism whereby FOP-mutant *ACVR1* drives HO and other phenotypes in FOP, we generated a genetically accurate mouse model by knocking in the most common FOP-causing variant of *ACVR1*, *ACVR1*[R206H]. To avoid the perinatal lethality observed with an unregulated knockin mouse line of *ACVR1*[R206H] (7), we employed a "conditional-on" strategy as described previously (8). The resulting mouse model of FOP, *Acvr1*^{[R206H]^{FIE}/+}; *GT(ROSA26)Sor*^{CreERT2/+}, is genotypically rendered FOP by systemic treatment with tamoxifen to activate CreER^{T2} and convert the *Acvr1*^{[R206H]^{FIE}} allele to *Acvr1*^{R206H}. HO is triggered by soft tissue trauma. Using this

► **Related Commentary:** <https://doi.org/10.1172/JCI160773>

Authorship note: SA and LH contributed equally to this work. ANE, VI, and SJH contributed equally to this work.

Conflict of interest: SA, LH, LW, ND, SR, YR, QZ, NR, KCN, VK, SB, LJ, SF, JLS, AJM, ANE, VI, and SJH are employees of Regeneron Pharmaceuticals and either own or have owned stock in Regeneron Pharmaceuticals. KS is an employee of Adimab, LLC, and holds shares in Adimab, LLC. PB is a cofounder of Keros Therapeutics, which develops therapeutics for hematological and musculoskeletal diseases that target TGF- β signaling pathways and is compensated for work on the company's scientific advisory board and owns equity in the publicly traded company. PB's interests are reviewed and managed by Brigham and Women's Hospital in accordance with their conflict-of-interest policies.

Copyright: © 2022, Aykul et al. This is an open access article published under the terms of the Creative Commons Attribution 4.0 International License.

Submitted: August 5, 2021; **Accepted:** April 28, 2022; **Published:** June 15, 2022.

Reference information: *J Clin Invest.* 2022;132(12):e153792.
<https://doi.org/10.1172/JCI153792>.

model, we demonstrated that HO in FOP requires activation of FOP-mutant ACVR1 by activin A (8). Furthermore, we demonstrated that activin A normally functions as an antagonist of BMP signaling via wild-type (WT) ACVR1, whereas it is perceived by FOP-mutant ACVR1 as an agonist and activates signaling just like a BMP (8, 9). Inhibition of activin A using a monoclonal antibody (mAb) completely abrogates the occurrence of new HO lesions and halts growth of nascent HO lesions, demonstrating that activation of FOP-mutant ACVR1 by activin A is required for HO in FOP mice (8, 10). These results have been independently reproduced (11–13), firmly establishing the requirement of activin A as an obligate factor for HO in FOP.

The finding that HO in FOP is ligand dependent suggested that antibodies that block ligand-induced activation of ACVR1 could be efficacious despite the disease-causing mutation being in the intracellular domain of this receptor. We therefore developed antibodies against ACVR1 that block ligand-induced signaling and tested whether such antibodies can inhibit HO in FOP mice. Surprisingly, although these anti-ACVR1 antibodies block ligand-induced signaling *in vitro*, they activate FOP-mutant ACVR1 and exacerbate (rather than block) HO in FOP mice. Careful investigation of signaling in cells where ACVR1 is not overexpressed revealed that anti-ACVR1 antibodies activate Smad1/5/8 phosphorylation when they dimerize FOP-mutant ACVR1, whereas they fail to activate Smad1/5/8 phosphorylation when they dimerize WT ACVR1. Hence, in cells that are genotypically FOP, anti-ACVR1 antibodies mimic the effects of activin A. The ability of anti-ACVR1 antibodies to activate FOP-mutant ACVR1 is independent of ligands but requires the presence of type II receptor ACVR2A or ACVR2B. Moreover, other means of dimerization of ACVR1 have the same effect as the anti-ACVR1 antibodies, suggesting that FOP-mutant ACVR1 is activated by simple dimerization (whereas WT ACVR1 is not). Similar results have been concurrently reported, thereby corroborating our observations (14). Activation of FOP-mutant ACVR1 in response to antibody-mediated dimerization mimics the response to activin A. More importantly, these results indicate that anti-ACVR1 antibodies should not be considered as a therapeutic strategy in FOP.

Results

ACVR1-blocking antibodies inhibit ligand-induced signaling through both WT ACVR1 and ACVR1[R206H] in vitro. Given the high level of amino acid sequence identity between mouse and human ACVR1, we utilized an *in vitro* yeast-based platform (15) to isolate human-murine ACVR1 cross-reactive antibodies. Three lead antibodies — mAb 1, mAb 2, and mAb 3 — were selected, as they display a high affinity for both human and mouse ACVR1 (Supplemental Tables 1 and 2; supplemental material available online with this article; <https://doi.org/10.1172/JCI153792DS1>), lack binding to related BMP receptors (Supplemental Table 3), and block signaling. We utilized 2 different assays as surrogates of Smad1/5/8 signaling: HEK293 cells (human embryonic kidney cells) harboring a BRE-luciferase reporter (9, 16) and alkaline phosphatase (ALP) activity (17). All 3 anti-ACVR1 mAbs block BMP7- and activin A-induced signaling in HEK293 cells overexpressing ACVR1[R206H], as measured by BRE-luciferase activity (Figure 1, A–C), as well as BMP7-induced Smad1/5/8 signaling, as measured by ALP activity in W20

cells (mouse bone stromal cells) overexpressing WT ACVR1 (Supplemental Figure 1, A and B).

ACVR1-blocking antibodies increase HO in FOP mice. We have previously demonstrated that activin A signaling through ACVR1[R206H] is required for HO in FOP mice and that its inhibition completely abrogates the initiation and progression of HO (8). We therefore reasoned that anti-ACVR1 antibodies that block ligand-induced signaling through ACVR1[R206H] should also be efficacious in this model. Unexpectedly, when anti-ACVR1 antibodies were dosed prophylactically at the time of initiation of the model, HO was greatly enhanced compared with the level of HO observed in FOP mice treated with an isotype control antibody (Figure 1, D and E). This suggested that these antibodies were activating rather than blocking the FOP-mutant ACVR1 *in vivo*. This property was shared by all 3 mAbs. Since these mAbs bind ACVR1 at different epitopes (Supplemental Table 4), the ability of these mAbs to exacerbate HO in FOP is a shared property of these antibodies and does not depend on binding ACVR1's extracellular domain at any particular site.

Anti-ACVR1 antibodies block trauma-induced HO in WT mice. To confirm that anti-ACVR1 antibodies can inhibit WT ACVR1 in the setting of HO *in vivo*, we tested whether mAb 1 is efficacious in the burn tenotomy model of trauma-induced HO (tHO) in WT mice (18). Consistent with previous data (19), either mAb 1 or ALK3-Fc (which blocks osteogenic BMPs) was able to reduce, though not completely ameliorate, tHO when dosed at the same time as induction of the model via burn combined with tenotomy (Supplemental Figure 2). These results confirm that antibody-mediated inhibition of WT ACVR1 blocks HO but only outside of FOP.

Effect of anti-ACVR1 antibodies on iron homeostasis in FOP mice is consistent with activating ACVR1[R206H]. We next tested whether this apparent activation of ACVR1[R206H] by anti-ACVR1 antibodies extends to other tissues, rather than being limited to HO. For this, we focused on iron homeostasis, where the role of ACVR1 is well established (20). Hence, we measured the effect of anti-ACVR1 antibodies on iron homeostasis using hepcidin levels as a surrogate, as well as serum iron levels directly. Hepcidin is a direct target of ACVR1 activation *in vivo*; hepcidin expression is upregulated by BMP2 and BMP6 signaling through ACVR1/BMPRIA in hepatocytes (20–22). Inhibition of ACVR1-mediated signaling is expected to decrease hepcidin levels (and increase serum iron), whereas its activation is expected to increase hepcidin levels (and decrease serum iron). We therefore used hepcidin production by the liver, as measured by circulating hepcidin levels, to determine the effect of anti-ACVR1 antibodies on ACVR1-mediated signaling. *Acvr1^{+/+}; GT(ROSA26)Sor^{CreERT2/+}* (WT) or *Acvr1^{[R206H]/+}; GT(ROSA26)Sor^{CreERT2/+}* (FOP) mice were dosed with mAb 1 and circulating hepcidin was measured. Treatment with mAb 1 resulted in a decrease in hepcidin in WT mice (Figure 2A), whereas it increased hepcidin levels in FOP mice (Figure 2B). The results obtained with hepcidin were mirrored by serum iron levels (Figure 2, C and D). These data demonstrate that the same anti-ACVR1 antibody inhibits WT ACVR1 but activates ACVR1[R206H] *in vivo* and extends its physiological effects to a system other than HO.

FOP-mutant ACVR1 is activated when artificially dimerized. We surmised that the most likely explanation for our results is that FOP-mutant ACVR1 is activated by simple dimerization, independently of

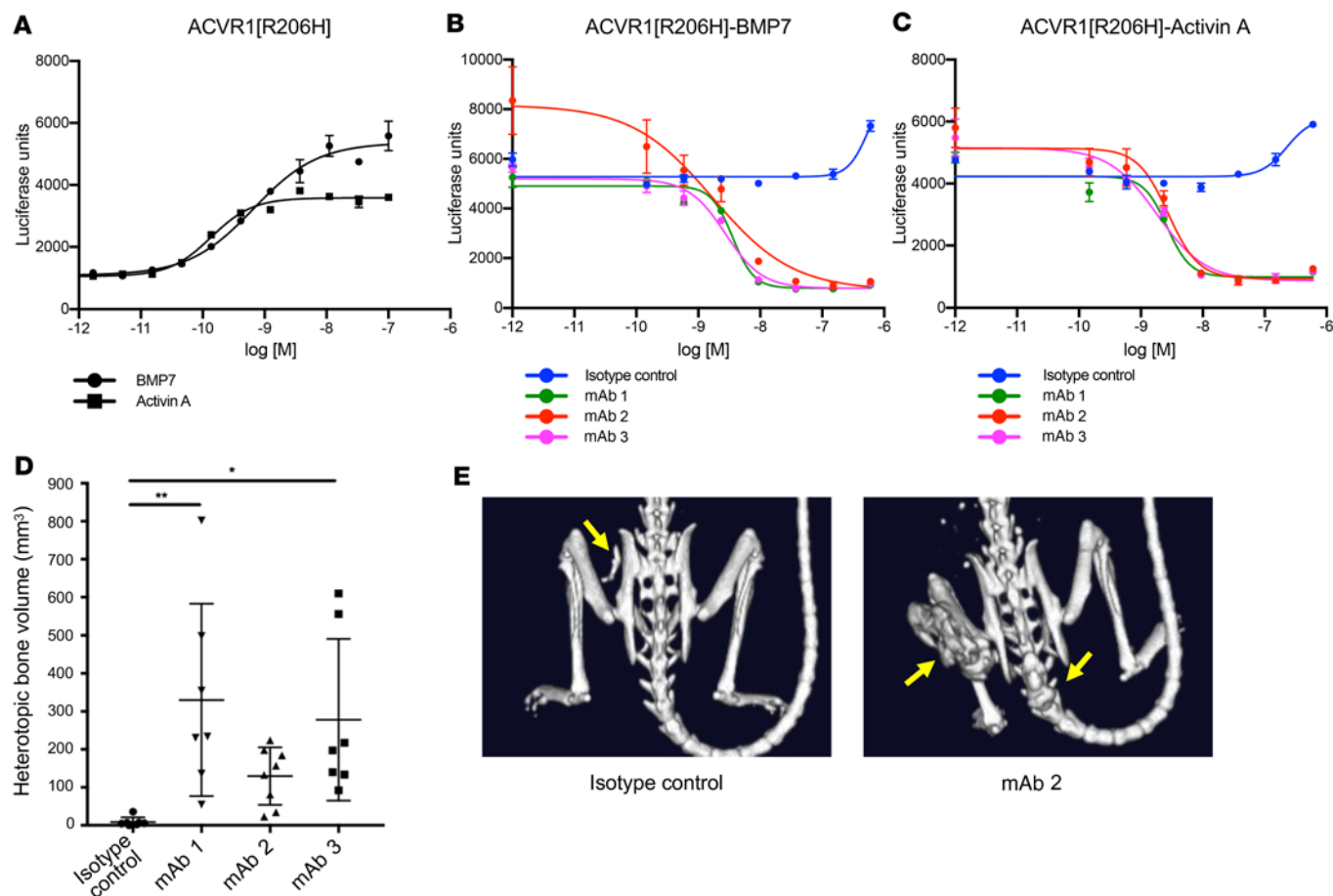


Figure 1. Anti-ACVR1 antibodies block BMP7 and activin A signaling in HEK293.ACVR1[R206H] cells but increase heterotopic bone formation in FOP mice. Activin A and BMP7 dose response was evaluated in stable pools of HEK293/BRE-luciferase reporter cells overexpressing ACVR1[R206H] (A). HEK293/BRE-luciferase reporter cells overexpressing ACVR1[R206H] were treated with a fixed concentration (2 nM) of BMP7 (B) or activin A (C). Anti-ACVR1 antibodies inhibited Smad1/5/8 phosphorylation induced by BMP7 or activin A (B and C). Data show the mean ($n = 4$) \pm SEM. Three biological replicates were performed for the in vitro signaling assays. (D) *Acvr1*^{[R206H]^{FIE}/+}; *GT(ROSA26)Sor*^{CreERT2}/+ mice were injected with tamoxifen to initiate the model and concurrently injected with anti-ACVR1 antibodies or isotype control antibody at 10 mg/kg weekly ($n = 7$ –8/group). Total heterotopic bone lesion volume was measured 4 weeks after initiation. Data show the mean \pm SD. * $P < 0.05$, ** $P < 0.01$ by 1-way ANOVA with Dunnett's multiple-comparison test. (E) Representative μ CT images of FOP mice [*Acvr1*^{[R206H]^{FIE}/+}; *GT(ROSA26)Sor*^{CreERT2}/+ after tamoxifen] treated with anti-ACVR1 antibody or isotype control antibody. Yellow arrows indicate the positions of heterotopic bone lesions.

its natural ligands, whereas WT ACVR1 is only activated in response to BMPs. To test this hypothesis, we utilized an artificial method of inducible dimerization, one that utilizes a small molecule-controlled dimerization domain, DmrB (23). We generated cells expressing either WT human ACVR1 or human ACVR1[R206H] bearing a DmrB domain fused to their C-termini. After demonstrating that each fusion retains its response to physiological ligands (i.e., BMP6 for WT ACVR1-DmrB and ACVR1[R206H]-DmrB, and activin A for ACVR1[R206H]-DmrB) (Figure 3, A and B), we tested their response to a small molecule dimerizer. Whereas WT ACVR1-DmrB failed to respond, dimerization of ACVR1[R206H]-DmrB activated signaling (Figure 3, C and D). The signal remained unaltered when ACVR2B-Fc (which would bind any endogenous ligands that might be present) was included, indicating that the observed response is not dependent on any endogenous ligands (Figure 3D). These results further highlight the fact that simple dimerization of ACVR1[R206H] activates that receptor, in stark contrast to WT ACVR1 whose activation requires interaction with specific BMPs.

Anti-ACVR1 mAbs activate, whereas Fabs block, ACVR1[R206H] signaling. The fact that simple, ligand-independent activation of FOP-mutant ACVR1 by dimerization activates this receptor lends credence to the idea that anti-ACVR1 antibodies induce signaling from this receptor by dimerizing it. Hence, we surmised that monovalent versions of anti-ACVR1 antibodies (which would be incapable of driving dimerization of ACVR1) should block activation of both ACVR1[R206H] and WT ACVR1. To test this idea, we generated fragment antigen-binding regions (Fabs) of 2 of the anti-ACVR1 antibodies (mAb 2 and mAb 3), Fab 2 and Fab 3, established that they block ligand-induced ACVR1-mediated signaling in vitro (Supplemental Figure 1, C and D, and Supplemental Figure 3), and then tested whether they can stop HO in FOP mice. To overcome the short in vivo half-life of Fabs, we used hydrodynamic delivery (HDD) to deliver plasmids encoding the Fabs to hepatocytes, hence enabling continuous production of the Fabs. These 2 Fabs significantly reduced HO in FOP mice (Figure 4, A and B) compared with a control antibody, thereby confirming that anti-ACVR1 Fabs can inhibit ACVR1[R206H] in vivo.

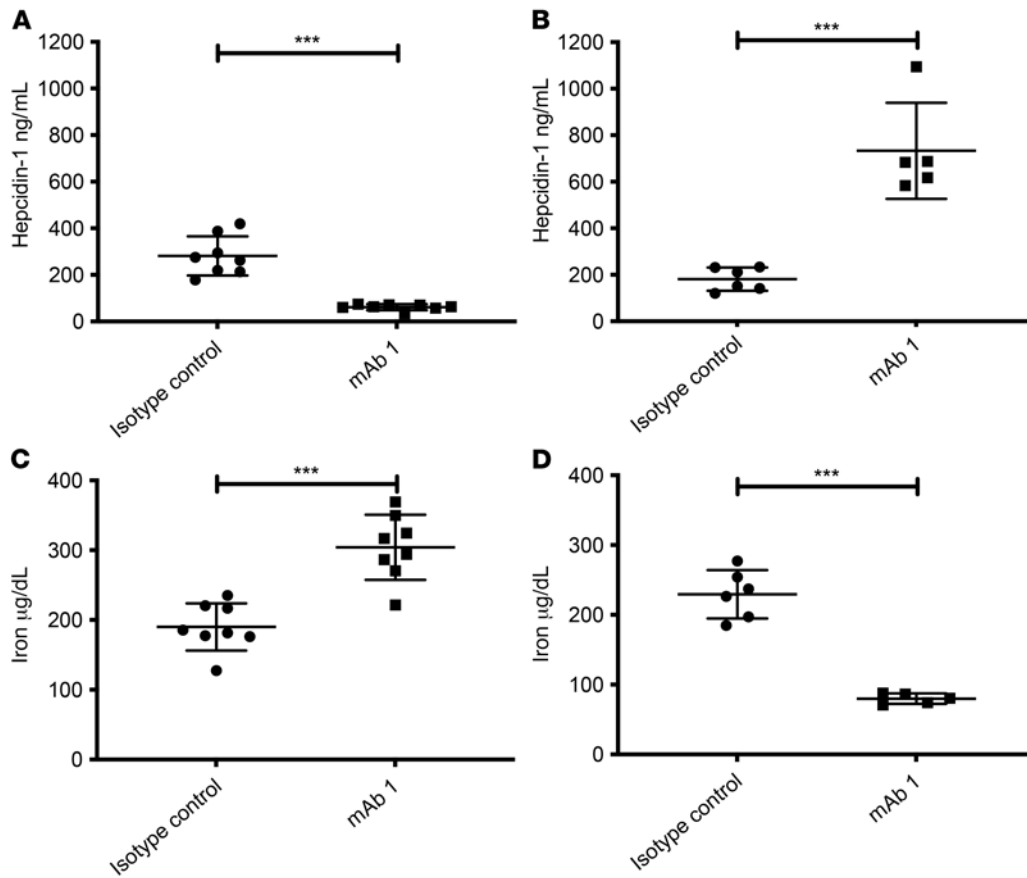


Figure 2. Anti-ACVR1 antibody-induced changes in hepcidin and iron levels are consistent with inhibition of WT ACVR1 and activation of ACVR1[R206H] in vivo. (A and C) In WT mice ($n = 8/\text{group}$), anti-ACVR1 mAb 1 decreased serum hepcidin (A) and increased serum iron (C). (B and D) In FOP mice [$Acvr1^{R206H/FlEx/+}; GT(ROSA26)Sor^{CreERT2/+}$, after tamoxifen] ($n = 5\text{--}6/\text{group}$), anti-ACVR1 mAb 1 increased serum hepcidin (B) and decreased serum iron (D). *** $P < 0.001$ by Student's t test.

In parallel with these in vivo experiments, we explored the effect of an anti-ACVR1 mAb and the corresponding Fab directly on signaling in vitro, focusing on 2 types of cells with endogenous expression of ACVR1: $Acvr1^{R206H/+}; GT(ROSA26)Sor^{CreERT2/+}$ mouse embryonic stem (mES) cells and fibroadipogenic progenitor cells (FAPs), i.e., the cells that give rise to HO in FOP mice (12, 13). Consistent with the in vivo data, mAb 2 was able to induce Smad1/5/8 phosphorylation in the absence of exogenously added ligand, albeit to a lower level than activin A (Figure 4C and Supplemental Figure 4). In contrast, mAb 2 could not induce Smad1/5/8 signaling in cells expressing WT ACVR1 (Supplemental Figure 5). As expected, Fab 2 failed to activate Smad1/5/8 signaling in ACVR1[R206H]-expressing cells but was able to block activin A-induced signaling. Identical results were obtained with another FOP-causing variant, ACVR1[R258G] (ref. 24 and Supplemental Figure 5). These results firmly establish that FOP-mutant ACVR1 is activated when dimerized by anti-ACVR1 antibodies, resulting in a signal that is lower than that obtained by activin A, but adequate to exacerbate HO and reduce serum iron in FOP mice.

Anti-ACVR1 antibody-induced activation of ACVR1[R206H] is independent of activin A. Given that the anti-ACVR1 antibodies block interaction of ACVR1 with its ligands, we considered it unlikely that the anti-ACVR1 antibody-induced signaling involves

activin A, the obligate ligand for HO in FOP. Nonetheless, to exclude this possibility we tested whether antibody activation of ACVR1[R206H] is dependent on activin A both in cells and in FOP mice. In both mES cells and FAPs the ability of mAb 2 to activate signaling was activin A independent (Figure 4C and Supplemental Figure 4), as treatment of these cells with both an activin A-blocking antibody and mAb 2 resulted in Smad 1/5/8 phosphorylation to similar levels as mAb 2 alone. To confirm that HO observed in FOP mice treated with anti-ACVR1 antibodies is independent of activin A, we tested whether anti-ACVR1 antibody-exacerbated HO persisted in FOP mice in the presence of activin A-blocking antibodies. Two anti-activin A antibodies were investigated: REGN2476, which blocks binding of activin A to both type I and type II receptors, and REGN2477, which allows binding of activin A to type II receptors but inhibits signaling

by blocking engagement with type I receptors (ref. 9 and Supplemental Figure 6). Both of these antibodies completely inhibit HO in FOP mice when dosed prophylactically (refs. 8, 10, and Figure 4D). However, neither of these antibodies was able to ameliorate the increased HO seen with the anti-ACVR1 antibody, demonstrating that this outcome is independent of activin A (Figure 4D).

Anti-ACVR1 antibody-induced activation of ACVR1[R206H] requires type II receptors. The fact that FOP-mutant ACVR1 can be activated by dimerization mediated by anti-ACVR1 antibodies even in the absence of extracellular ligands (Figure 4) prompted us to investigate whether type II receptors play a role in this process. For these experiments, we engineered $Acvr1^{R206H/+}; GT(ROSA26)Sor^{CreERT2/+}$ mES cell lines lacking $Acvr2a$ and $Acvr2b$, or $Bmpr2$, or all 3 of these type II receptor genes. Prior to use, these mES cell lines were tested for expression of ACVR1, ACVR2A, ACVR2B, and BMPR2 (Supplemental Figures 7 and 8), in order to ascertain that the expression of these genes was not altered except as intended. Subsequently, these mES cell lines were treated with activin A or BMPs or the anti-ACVR1 antibody mAb 1. Loss of BMPR2 did not have any appreciable effect on signaling either by ligands or mAb 1. However, loss of ACVR2A and ACVR2B rendered these cells unresponsive to activin A as well as mAb 1 (Figure 5A), indicating that type II receptors are required for signaling beyond

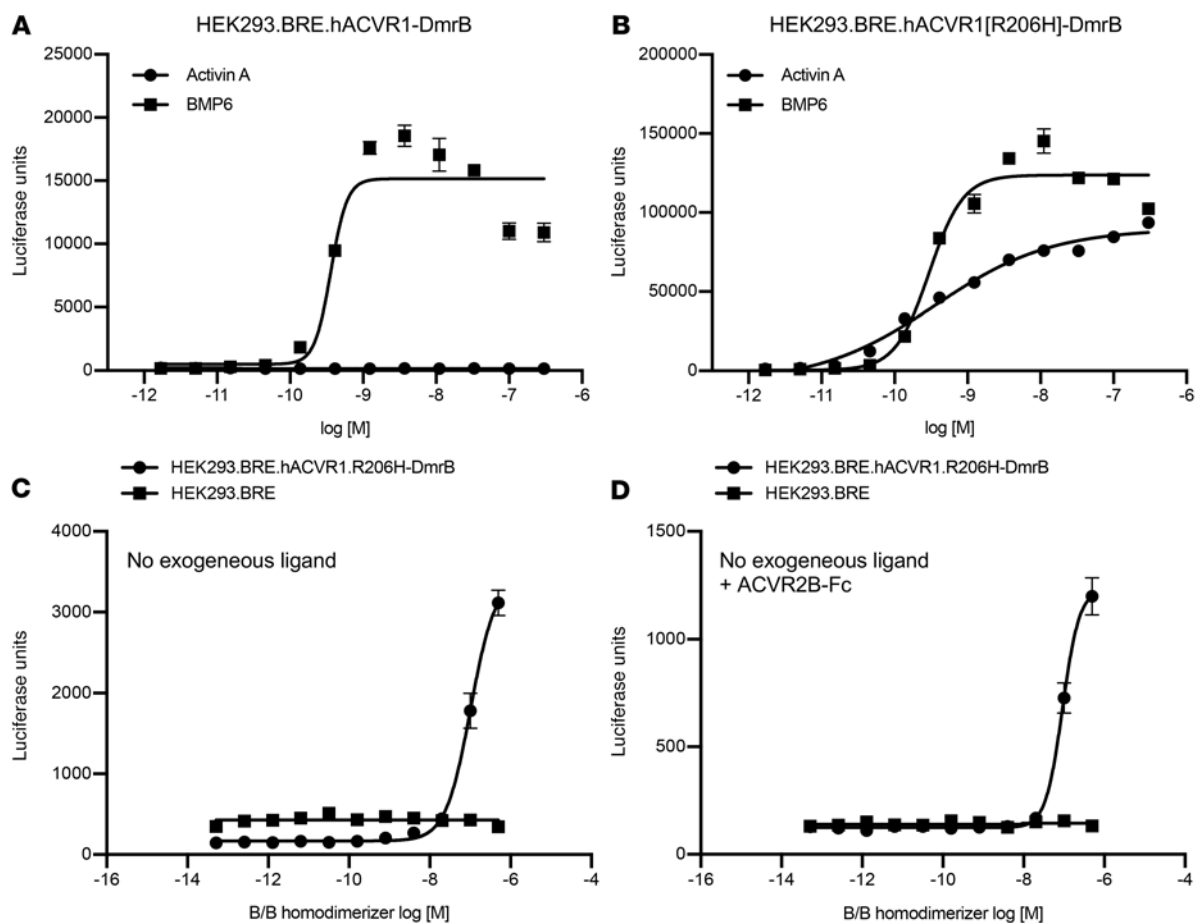


Figure 3. Ligand-independent dimerization of ACVR1[R206H], but not WT ACVR1, induces Smad1/5/8 signaling. HEK293 cells harboring p-Smad1/5/8-responsive luciferase reporter (BRE) were transfected with hACVR1-DmrB (**A**) or hACVR1[R206H]-DmrB (**B**). Homodimerization of C-terminally DmrB-tagged ACVR1 was induced with 20 nM B/B homodimerizer for 16 hours. Activin A activated Smad1/5/8 signaling only in hACVR1[R206H]-DmrB cells, but BMP6 activated Smad1/5/8 signaling both in hACVR1-DmrB and hACVR1[R206H]-DmrB cells (**A** and **B**). Intracellular homodimerization of hACVR1[R206H] activated Smad1/5/8 signaling in the absence of exogenous ligands (**C**) as well as in the presence of 300 nM ACVR2B-Fc ligand trap (**D**). Data show the mean ($n = 4$) \pm SEM. Three biological replicates were performed for the in vitro signaling assays.

ligand presentation to ACVR1. Our results agree with published reports that type II receptors are required for signaling by ACVR1, independent of ligand binding (25–27).

This result also suggested that type II receptors must exist in preformed heterodimeric complexes with ACVR1. Such complexes indeed exist, as immunoprecipitation of a Myc-tagged ACVR1 coimmunoprecipitates ACVR2B (Figure 5B and Supplemental Figure 9). These preformed complexes are not specific to ACVR1[R206H], as they also form with WT ACVR1. Similar preformed heterodimeric complexes have been observed between other type I and type II BMP receptors (28), and hence appear to be a general property of this class of receptors.

Anti-ACVR1 antibodies also activate human ACVR1[R206H]. Human and mouse ACVR1 differ by 5 amino acids in their mature form (Supplemental Figure 10). Two of these amino acids are found in the intracellular domain, specifically at positions 182 and 330. It has been reported that the amino acid at position 330 is a key determinant of the response of ACVR1 to anti-ACVR1 antibodies in vitro, and more specifically that proline at position 330 renders human ACVR1[R206H] resistant to activation by

dimerization (29). This stands in contrast to mouse ACVR1, which has a serine at position 330.

To investigate this reported difference in vivo, we changed serine 330 to proline and humanized the extracellular domain (huccto) of *Acvr1*^{[R206H]FIE_x} to produce *Acvr1*^{huccto[R206H]FIE_x;[S330P]^{+/+}}; *GT(ROSA26)Sor^{CreERT2}/+* mES cells and mice. As with the original mouse model, we induced the FOP genotype in mice through treatment with tamoxifen to generate their FOP counterparts (FOP^[S330P] mice). We then dosed both FOP and FOP^[S330P] mice with mAb 1 simultaneously with initiation of the model. As expected, mAb 1 induced severe HO in FOP mice that necessitated that they be euthanized after 3 weeks. In FOP^[S330P] mice, anti-ACVR1 antibody treatment also increased HO compared with isotype control, albeit to a lower level than that seen in FOP mice (Figure 6, A and B). This difference in degree of activation was mirrored in the change in serum iron levels, which were more reduced in FOP mice than in FOP^[S330P] mice (Supplemental Figure 11). Nonetheless, both effects — an increase in HO and a decrease in serum iron — were observed with mAb 1 treatment of FOP^[S330P] mice, mirroring the results obtained with FOP mice.

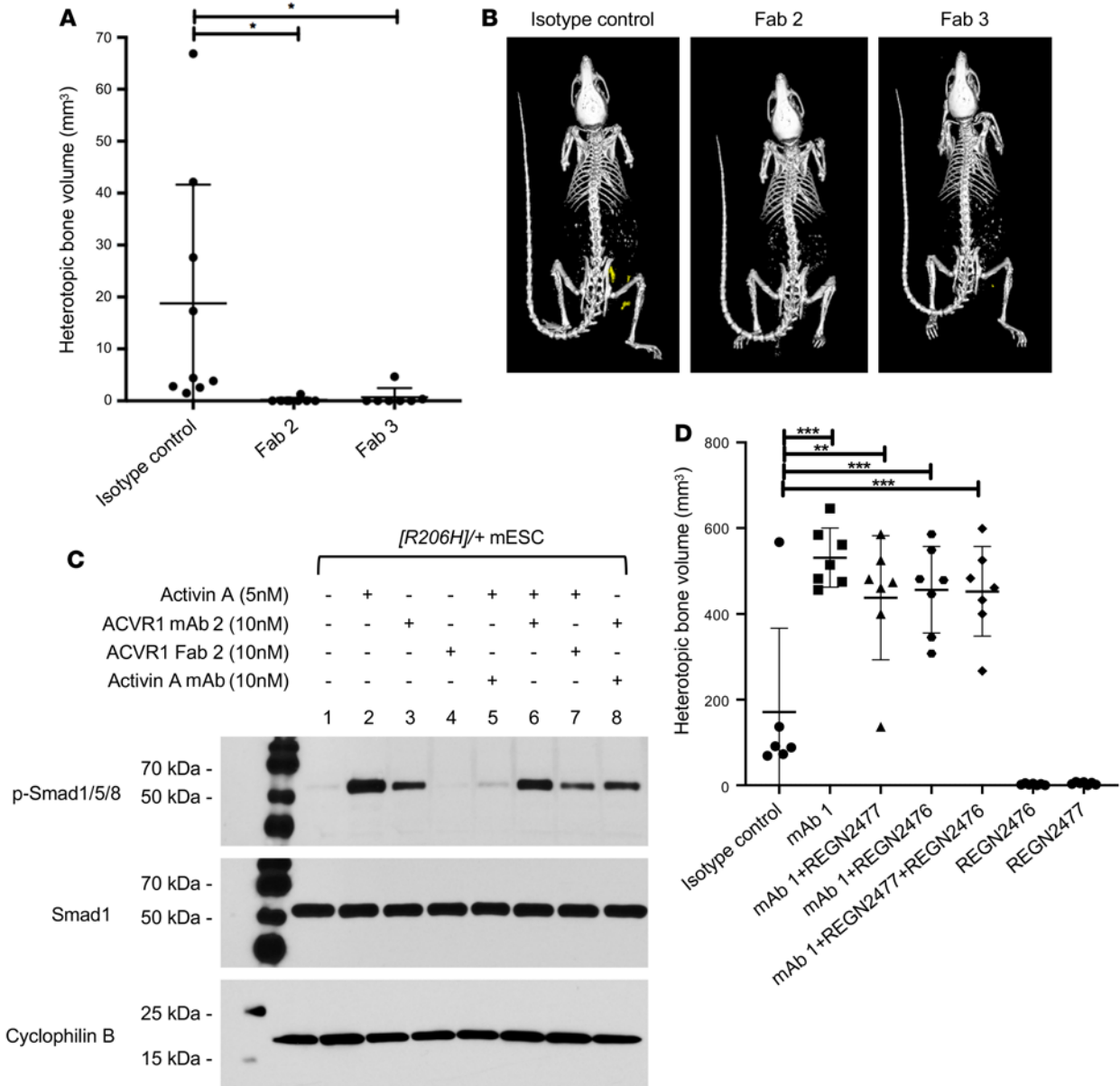


Figure 4. Dimeric anti-ACVR1 antibodies activate, whereas monomeric anti-ACVR1 Fabs block, ACVR1[R206H]. (A) *Acvr1*^{[R206H]^{FIE}/+}; *GT*(*ROSA26*)*Sor*^{CreERT2/+} mice (*n* = 7–9/group) received plasmids expressing anti-ACVR1 Fabs or a plasmid encoding a control mAb by hydrodynamic delivery (HDD) 5 days after initiation of the model with tamoxifen. HO was triggered in the hind limb by muscle pinch 7 days after HDD and total heterotopic bone volume was measured 6 weeks after injury. FOP mice [*Acvr1*^{[R206H]^{FIE}/+}; *GT*(*ROSA26*)*Sor*^{CreERT2/+}, after tamoxifen] expressing anti-ACVR1 Fab showed reduced HO compared with control mice. Data show the mean ± SD. **P* < 0.05 by 1-way ANOVA with Dunnett’s multiple-comparison test. (B) Representative μCT images of FOP mice expressing either anti-ACVR1 Fab or an isotype control antibody. (C) *Acvr1*^{[R206H]/+}; *GT*(*ROSA26*)*Sor*^{CreERT2/+} ([R206H]/+) mES cells (mESC) were treated with activin A, anti-ACVR1 mAb 2, anti-ACVR1 Fab 2, or anti-activin A mAb (REGN2476) in various combinations for 1 hour. Activin A and anti-ACVR1 mAb 2 but not anti-ACVR1 Fab 2 induced Smad1/5/8 phosphorylation. Anti-ACVR1 Fab 2 significantly reduced activin A–induced Smad1/5/8 phosphorylation, whereas anti-ACVR1 mAb 2 only slightly reduced activin A–induced Smad1/5/8 phosphorylation. (D) Anti-ACVR1 antibody activation of ACVR1[R206H] is independent of activin A. *Acvr1*^{[R206H]^{FIE}/+}; *GT*(*ROSA26*)*Sor*^{CreERT2/+} mice (*n* = 6–8/group) were injected with tamoxifen to initiate the model and concurrently injected with antibodies at 10 mg/kg weekly. Total heterotopic bone volume was measured 3 weeks after initiation. Data show the mean ± SD. **P* < 0.05, ***P* < 0.01, ****P* < 0.001 by 1-way ANOVA with Dunnett’s multiple-comparison test.

However, in vitro, the antibody-induced dimerization of ACVR1[huceto;R206H;S330P] did not result in detectable levels of Smad1/5/8 phosphorylation, when mAb 1 was the dimerizing antibody. We attributed this to the fact that mAb 1 recognizes both the WT and FOP mutant allele and therefore induces dimeric complexes of WT/WT, WT/FOP, and FOP/FOP ACVR1, and hence

potentially resulting in a situation where only 25% of FOP-mutant ACVR1 would transduce signal. We reasoned that an anti-ACVR1 antibody that recognizes only human ACVR1 (Supplemental Tables 1 and 2) and hence promotes solely the formation of ACVR1[huceto;R206H;S330P] homodimers would elevate the level of signaling to the point that it can be detected. Indeed, using such an antibody

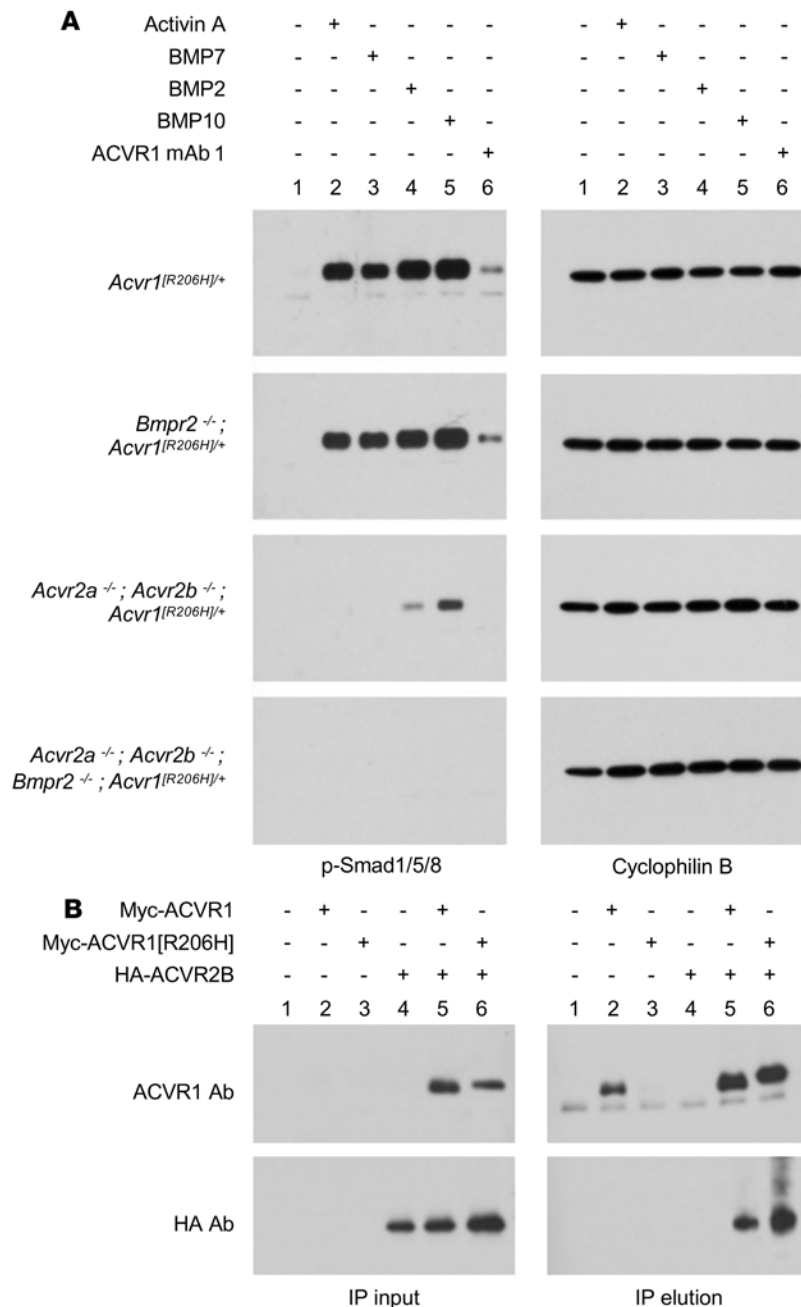


Figure 5. Anti-ACVR1 antibody activation of ACVR1[R206H] is type II receptor dependent. (A) *Acvr1^{[R206H]/+}; GT(ROSA26)Sox^{CreERT2/+} ([R206H]/+)* mES cells lacking *Acvr2a* plus *Acvr2b*, or *Bmpr2* or all 3 of these type II receptor genes were treated with 10 nM activin A, BMP7, BMP2, BMP10, or anti-ACVR1 mAb 1 for 1 hour. Activin A, BMP7, BMP2, BMP10, and anti-ACVR1 mAb 1 induced Smad1/5/8 phosphorylation in cells that lack *Bmpr2* but retain *Acvr2a* and *Acvr2b*, but not in cells where *Acvr2a* and *Acvr2b* or all 3 type II receptors have been knocked out. (B) ACVR2B coimmunoprecipitates with both ACVR1 and ACVR1[R206H] from W20 cells expressing Myc-tagged ACVR1 and/or HA-tagged ACVR2B. Myc-ACVR1 was immunoprecipitated using an anti-Myc antibody. ACVR1 and ACVR2B were detected using an anti-ACVR1 or anti-HA antibody, respectively.

as the dimerizing antibody resulted in induction of Smad1/5/8 phosphorylation (Figure 6C). This result is consistent with that obtained when dimerizing human ACVR1[R206H]-DmrB (Figure 3, C and D). Hence, these results indicate that the property of

ACVR1[R206H] to be activated when dimerized by anti-ACVR1 antibodies is conserved between human and mouse ACVR1. Although it appears that human ACVR1[R206H] is less active than its mouse counterpart, these results strongly caution against the use of anti-ACVR1 antibodies as therapeutic agents to block HO in FOP, because they clearly induce more HO than that observed when FOP^[S330P] mice are dosed with a control antibody (akin to placebo) and they may even induce anemia.

Discussion

In our quest to develop disease-modifying therapies for FOP, we sought to understand how FOP-mutant ACVR1 drives HO. We engineered a genetically accurate mouse model of FOP and have relied on this model to explore the pathophysiology of FOP and place findings from in vitro experiments in a physiological context. Using this approach, we discovered an unusual property of FOP-mutant ACVR1, i.e., that it is activated by its own natural antagonist, activin A (8). Whereas WT ACVR1 forms nonsignaling complexes with activin A and the corresponding type II receptors (9), FOP-mutant ACVR1 is activated by activin A. This neofunction is essential for HO in FOP, as inhibition of activin A using mAbs ameliorates the initiation and progression of heterotopic bone lesions in FOP mice (8, 10, 13). These results culminated in a clinical trial — LUMINA-1 (ClinicalTrials.gov NCT03188666) — to test the safety and efficacy of REGN2477 (an anti-activin A mAb) in FOP.

In addition, these results unequivocally demonstrated the ligand dependence of HO in FOP (with the “culprit” ligand being activin A). Based on this, we reasoned that inhibition of ligand-induced signaling using antibodies against ACVR1 may present an additional potential therapeutic approach. To this effect, we generated a set of anti-ACVR1 mAbs that block signaling from ACVR1 in vitro. Surprisingly, these mAbs exacerbate HO in FOP mice, and activate Smad1/5/8 phosphorylation in cells expressing FOP-mutant ACVR1 in vitro, in the absence of ligands. Furthermore, this effect is not restricted to HO, as anti-ACVR1 antibodies also alter iron homeostasis in a manner consistent with activation of ACVR1[R206H]; they increase hepcidin levels and reduce serum iron levels, phenocopying activation of signaling via ACVR1.

At first glance, these results contradict our initial bioassay data (Figure 1), where we utilized cells overexpressing ACVR1[R206H] and a BRE-luciferase assay as a surrogate for activation of the

Smad1/5/8 pathway to screen for mAbs with the desired properties. Such a discrepancy has been noted by others (27). Our results demonstrating that ACVR1 exists in preformed and ligand-independent heterocomplexes with its corresponding type II receptors

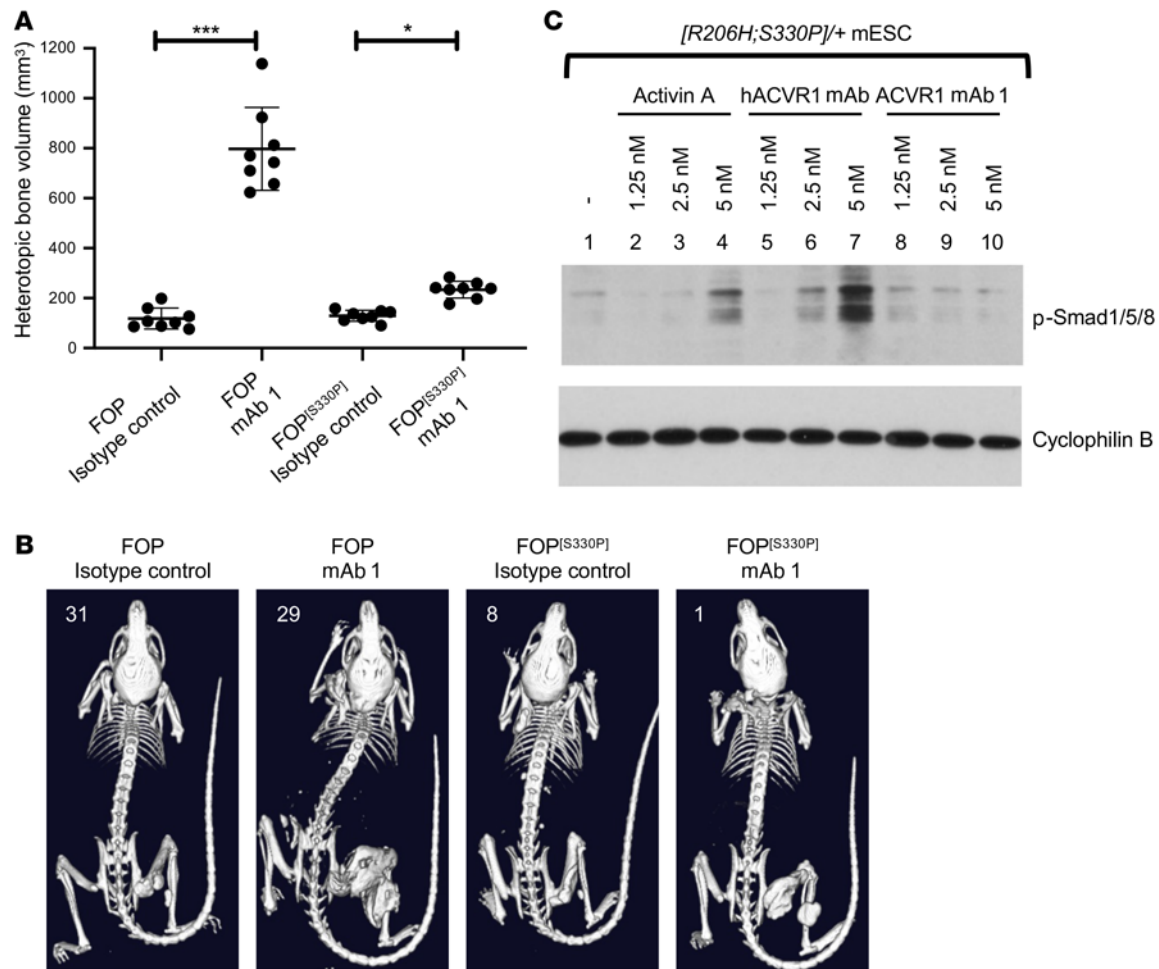


Figure 6. ACVR1[R206H;S330P] is activated by anti-ACVR1 antibodies but to a lesser degree than ACVR1[R206H]. (A and B) *Acvr1*^{[R206H]^{FlEx/+}; *GT*(*ROSA26*)*Sor*^{*CreERT2/+*} mice or *Acvr1*^{[huecto;[R206H]^{FlEx};[S330P]^{+/+}]; *GT*(*ROSA26*)*Sor*^{*CreERT2/+*} (*FOP*^[S330P]) mice were injected with tamoxifen to initiate the model and concurrently injected with anti-ACVR1 mAb 1 or isotype control antibody at 10 mg/kg weekly ($n = 8$ /group). Total heterotopic bone volume was measured 3 weeks after initiation of the model. ACVR1 mAb 1 increased HO compared with isotype control in both mouse models, though to a lesser degree in *FOP*^[S330P] mice. Data show the mean \pm SD. * $P < 0.05$, *** $P < 0.001$ by 1-way ANOVA with Bonferroni's multiple-comparison test. (C) *Acvr1*^{[huecto;[R206H;S330P]^{+/+}]; *GT*(*ROSA26*)*Sor*^{*CreERT2/+*} (*[R206H;S330P]*^{+/+}) mES cells were treated with 10 nM activin A, anti-ACVR1 mAb 1, or anti-hACVR1 antibody and assessed for phosphorylated Smad1/5/8. Anti-hACVR1 mAb (that only binds ACVR1[huecto;R206H;S330P]) and not WT mouse ACVR1 induced Smad1/5/8 phosphorylation, whereas mAb 1 (which recognizes both human and mouse ACVR1) did not drive an appreciable level of Smad1/5/8 phosphorylation.}}}

provide a possible explanation for this discrepancy. Under over-expression conditions, where ACVR1 is expressed at much higher levels than those encountered in physiological settings, the majority of ACVR1 is unlikely to exist in preformed complexes with type II receptors (as the levels of type II receptors become limiting). Therefore, when anti-ACVR1 antibodies engage and dimerize FOP-mutant ACVR1, it is unlikely that the majority of resulting complexes are going to involve type II receptors and hence transduce signal. In contrast, when complex formation is driven by ligand, which requires engaging type II receptors first, signaling will not be affected, as the great majority of resulting complexes will include ACVR1. However, when anti-ACVR1 antibodies are included in addition to ligand, they outcompete ligand, and drive the formation of complexes much like those generated in the absence of ligand. Irrespective of the reasons for the discrepancy observed in signaling outcomes between our initial bioassay and our in vivo data, it is clear that in physiological settings ACVR1[R206H] is activated

by anti-ACVR1 mAbs. This observation has been concurrently and independently corroborated using a different anti-ACVR1 antibody and a different mouse model of FOP (14). Furthermore, at least in vitro, it also holds for an additional FOP-causing variant of ACVR1, 258G; however, we have yet to test any other ACVR1 variants documented to cause FOP (4).

Although the level of antibody-induced activation is well below that seen with ligand-induced activation, the antibodies greatly exacerbate HO in FOP mice. We postulate that this is due to a more widespread and sustained availability of an antibody, in contrast to a local and immediate but transient induction of activin A after muscle injury (30). We perhaps see evidence of this reflected in the characteristics of HO lesions in antibody-treated mice (Supplemental Figure 12). At 2 weeks after injury, HO lesions in anti-ACVR1 antibody-treated mice appear larger but less mature than those seen in isotype control-treated mice, suggesting that the initial injury-induced activin A signal is inhibited and replaced

with the weaker but more widespread antibody-induced signal in the injured muscle. However, subsequently in anti-ACVR1 antibody-treated mice the HO process remains far more active than in isotype control-treated mice, suggesting that the endogenous activin A signal has decreased but the anti-ACVR1 antibody is still abundant and, by activating FOP-mutant ACVR1, can continue to direct FAPs down an endochondral lineage (12, 13). Nevertheless, antibody-induced HO is indistinguishable from activin A-induced HO when analyzed histologically and shows the expected spectrum of cell types such as proliferating fibroblasts, chondrocytes, and mature bone (Supplemental Figure 13 and ref. 8).

Our data also support a requirement for some degree of muscle trauma that necessitates a repair response to initiate HO in FOP. This repair response is likely to be required not only to provide activin A but also to activate and expand FAPs so that they can respond to activin A and differentiate down an endochondral lineage. If activation of FAPs by injury were not required, then anti-ACVR1 antibodies would induce HO much more widely when administered to FOP mice, which is clearly not the case. These data are also consistent with the phenotype seen in the mouse model expressing ACVR1[Q207D], an engineered constitutively active and ligand-independent variant of ACVR1. In these mice, injury is also required to induce HO (31), indicating that ACVR1-mediated signaling leads to HO only if it takes place within cells that are primed to respond.

Activation of FOP-mutant ACVR1 by anti-ACVR1 mAbs is a result of dimerization of this receptor by these naturally bivalent mAbs. Consistent with this notion, anti-ACVR1 Fabs, which are naturally monovalent and hence cannot dimerize ACVR1, block HO in FOP mice very effectively and fail to activate ACVR1[R206H] *in vitro*. Further evidence that dimerization is adequate to activate FOP-mutant ACVR1 is that other methods of dimerization produce the same result. For example, activation is also achieved when an ACVR1[R206H]-DmrB fusion protein is dimerized by the corresponding small molecule. Furthermore, dimerization of an N-terminally Myc-tagged human ACVR1[R206H] using an anti-Myc antibody activates signaling, indicating that the dimerizing antibody need not bind to a region of ACVR1 that is involved in ligand engagement (data not shown).

The responsiveness of FOP-mutant ACVR1 to anti-ACVR1 antibodies is conserved between mouse and human ACVR1[R206H], contrary to an initial report that this might not be the case (29). This report attributed the apparent resistance of human ACVR1[R206H] to dimerization-induced activation to the presence of a proline at position 330, rather than serine in mouse ACVR1[R206H]. We show here that human ACVR1[R206H] is activated by anti-ACVR1 antibodies, but the resulting signal is weaker than that generated by mouse ACVR1[R206H]. In FOP^{S330P} mice, anti-ACVR1 antibodies exacerbate HO, though to a lesser degree than when engaging mouse ACVR1[R206H], mirroring the lower activity displayed by human ACVR1[R206H] *in vitro*.

Although activation of FOP-mutant ACVR1 by antibodies occurs in the absence of ligands, we demonstrate that type II receptors are still required. Type II receptors appear to be associated with ACVR1 (both WT and FOP-mutant) in preformed, ligand-independent complexes. Our findings mirror observations made for BMPR1A or BMPR1B and BMPR2 (28). Given that these complexes are not specific to FOP-mutant ACVR1, it remains unclear as to

why anti-ACVR1 antibodies do not also activate WT ACVR1. Hence, antibody-induced dimerization of ACVR1 appears to be equivalent to activin A-induced homodimerization of ACVR1; neither one activates WT ACVR1, whereas both activate FOP-mutant ACVR1.

Furthermore, our results clarify the role of activin A and FOP-mutant ACVR1 in inducing and supporting HO in FOP. Although our previous findings clearly established that activin A is the required ligand for HO in FOP (8), they did not address whether activation of ACVR1B (also known as ALK4) by activin A also plays a role in HO in this condition. Two pieces of evidence provided here conclusively demonstrate that activation of ACVR1B by activin A in FOP does not have an obligate role in the HO process. First, anti-ACVR1 antibodies alone can substitute for activin A in driving HO, which in turn indicates that induction of Smad1/5/8 signaling (and not Smad2/3) is what drives HO in FAPs. Second, HO induced by anti-ACVR1 antibodies in FOP mice cannot be blocked by anti-activin A antibodies, indicating that activation of Smad2/3 signaling via activin and ACVR1B must not be playing an obligate role in HO in FOP. Based on these observations, we conclude the required function of activin A in this process is to dimerize and activate FOP-mutant ACVR1 (Supplemental Figure 14).

Overall, our results indicate that FOP-mutant ACVR1 likely exists in a “permissive” conformation wherein it can be activated by simple dimerization. In physiological settings, ligands drive the formation of a tetrameric complex of 2 type I and 2 type II receptors to activate signaling. They do so by engaging the type II receptors and hence dimerizing preformed heterocomplexes of ACVR1 with its cognate type II receptors. In principle, dimerization of ACVR1 by anti-ACVR1 antibodies bypasses the requirement for ligand and type II receptors. However, our results clearly indicate that type II receptors are still required to activate signaling, as in their absence anti-ACVR1 antibodies do not activate FOP-mutant ACVR1. The reason that type II receptors are able to participate in signaling complex formation as brought about by anti-ACVR1 antibodies is because they exist in preformed (and ligand-independent) heterocomplexes with ACVR1 (Supplemental Figure 14). In spite of these insights, the molecular mechanism by which stoichiometrically identical complexes (i.e., ACVR1•activin A•type II receptor and ACVR1•ACVR1 mAb•type II receptor, both of which do not signal, versus ACVR1^{FOP}•activin A•type II receptor and ACVR1^{FOP}•ACVR1 mAb•type II receptor, or ACVR1•BMP•type II receptor, which transduce signal) result in these 2 opposite outcomes remains elusive.

Taken together, our results reveal an additional property of FOP-mutant ACVR1, i.e., that it is activated by anti-ACVR1 antibodies, which exacerbate rather than ameliorate HO in FOP mice. This property is limited to FOP-mutant ACVR1, as WT ACVR1 is not activated by said antibodies. Therefore, anti-ACVR1 antibodies may be considered as a potential therapeutic option for trauma-induced HO in non-FOP settings and could also be considered in conditions where increasing iron levels is desirable. However, given the catastrophic nature of HO in FOP, our results indicate that anti-ACVR1 antibodies should not be considered as a therapeutic option in this condition.

Methods

Reagents. Activin A (338-AC-500/CF), BMP2 (355-BM-100/CF), BMP7 (354-BP-010/CF), BMP10 (2926-BP-025/CF), and ACVR1B-Fc

(808-AR-100) were purchased from R&D Systems. Anti-ACVR1 Fabs were generated from corresponding anti-ACVR1 mAbs and purified in-house. Human ACVR1 (REGN3111) and mouse ACVR1 (REGN3407) ectodomain (amino acids 21–123).mmh (used in the binding experiments) were expressed and purified in-house. Anti-activin A antibodies (REGN2476 and REGN2477), anti-ACVR2A/B antibody, anti-Myc antibody (REGN642, used in the binding experiments), and hIgG4 isotype control antibody were expressed and purified in-house. ALK3 ectodomain (amino acids 24–152)-Fc and ACVR2B ectodomain (amino acids 23–133)-Fc soluble proteins were made in-house.

Antibody discovery and optimization. Human antibodies against ACVR1 (human and mouse cross-reactive) were isolated from a full-length human IgG synthetic naive library using an in vitro yeast selection system and associated methods (15). An antibody library of approximately 1×10^{10} in diversity was designed and propagated as described previously (15, 32). ACVR1-binding antibodies were enriched by incubation of biotinylated ACVR1-Fc and Myc-His monomeric ACVR1 at different concentrations with antibody-expressing yeast cells followed by magnetic bead selection (Miltenyi Biotec) or flow cytometry on a FACSAria II cell sorter (BD Biosciences) using fluorescent streptavidin or extravidin secondary reagents in several successive selection rounds. Antibodies cross-reactive to off-target proteins ALK1, ALK3, and ALK6 were actively depleted from selection outputs. After the last round of enrichment, yeast cells were plated onto agar plates, analyzed by DNA sequencing, and expanded for IgG production. Heavy chains from the naive outputs were used to prepare light-chain diversification libraries, which were then used for additional selection rounds. In particular, heavy chains were extracted from the fourth naive selection round outputs and transformed into a light-chain library consisting of 1×10^6 unique light chains to create new libraries approximately 1×10^8 in total diversity. Antibody optimization was completed in 3 phases. Optimization of the heavy chain via diversification of the complementarity-determining regions (CDRs) CDR-H1 and CDR-H2 followed either by mutagenic PCR-based diversification of the entire heavy chain variable region or diversification of the light chain CDR-L1 and CDR-L2 segments. CDR-H1 and CDR-H2 regions were diversified with premade libraries of CDR-H1 and CDR-H2 variants of a diversity of approximately 1×10^8 . Mutagenic PCR-based and premade libraries with CDR-L1 and CDR-L2 variants had diversities of approximately 1×10^7 and 1×10^5 , respectively. Lead variants were further diversified via DNA oligonucleotide sequence variegation of the CDR-H3 or CDR-L3. Oligonucleotide CDR-H3 and CDR-L3 libraries had a diversity of approximately 1×10^4 and 1×10^3 , respectively. Diversified antibody lineage populations were selected for enhanced binding to the target proteins while avoiding undesired cross-reactivity. The methods used for selections on diversified populations are similar or identical to those used to isolate the original lead IgGs (32). An additional anti-ACVR1 antibody that recognizes only human ACVR1 was also used in this study and has been previously described (19).

FOP mouse model. *Acvr1*^{R206H|FIEx/+} (*Acvr1*^{tm2.1VlCg}) and the accompanying Cre transgenic line, *Gt(ROSA26)Sor^{CreERT2/+}* (*Gt(ROSA)26Sor^{tm3.1(cre/ERT2)VlCg}*), used to generate *Acvr1*^{R206H|FIEx/+}; *Gt(ROSA26)Sor^{CreERT2/+}* mice have been previously described (8, 33). These were maintained in heterozygosity on a mixed C57BL/6NTac-129S6/SvEvTac background. Both male and female mice were used between 8 and 27 weeks of age; however, mice were matched for age and sex between groups. The model was initiated by inversion of the R206H-encoding exon into the sense

strand, which was accomplished by treating *Acvr1*^{R206H|FIEx/+}; *Gt(ROSA26)Sor^{CreERT2/+}* mice with 40 mg/kg of tamoxifen (Sigma-Aldrich) in oil intraperitoneally (i.p.) daily for 5 days (to activate CreER^{T2}). HO was initiated by pinch injury to the gastrocnemius muscle using a hemostat for 15 seconds. To assess HO, mice were anesthetized by isoflurane and whole-body scanned, with a field of view of 60 mm × 120 mm, using in vivo μ CT (Quantum FX, PerkinElmer). The X-ray source was set to a current of 160 μ A, voltage of 90 kVp, with a voxel size at 120 or 240 μ m.

Antibody dosing of mice. For treatment studies, mice were separated to ensure age and sex matching across groups, and treatments were initiated on the same day as tamoxifen administration. Antibodies against ACVR1 (mAb 1, mAb 2 and mAb 3), activin A (REGN2476 and REGN2477), and an hIgG4 isotype control were used in these studies. Mice were injected subcutaneously (s.c.) with 10 mg/kg antibodies twice weekly for the duration of the studies. Heterotopic bone lesions were visualized by in vivo μ CT imaging.

HDD of anti-ACVR1 Fabs. Anti-ACVR1 Fabs were delivered by HDD (34) 5 days after initiation of the model by tamoxifen. Briefly, 25 μ g of DNA plasmid encoding the CH1 and VH domains and 25 μ g of DNA plasmid encoding the CL and VL domains under the control of the ubiquitin promoter were diluted in 2 mL of PBS and injected into the tail vein in 5 to 7 seconds. HO was initiated in the hind limb by muscle pinch 7 days after HDD. Serum Fab concentration was measured 7 days after HDD by ELISA using a goat anti- κ light chain antibody (Thermo Fisher Scientific).

Serum hepcidin and iron measurements. Serum hepcidin was measured using a murine hepcidin ELISA kit (Intrinsic Biosciences) following the manufacturer's protocol. Serum iron was measured using the QuantiChrom Iron Assay Kit (BioAssay Systems, DIFE-250) following the manufacturer's protocol.

Fibro/adipogenic progenitor isolation and culture. Details of skeletal muscle dissection have been previously described (13). In brief, muscle was dissected from *Acvr1*^{R206H|FIEx/+}; *Gt(ROSA26)Sor^{CreERT2/+}* mice and dissociated using the Skeletal Muscle Dissociation Kit (Miltenyi Biotec) and gentleMACS Octo Dissociator with heaters (Miltenyi Biotec), in accordance with the manufacturer's instructions. Following centrifugation at 300g and 4°C for 10 minutes, the supernatant was discarded, and the pellet was resuspended in growth media (Dulbecco's modified Eagle medium (DMEM; Life Technologies) with 50 U/mL penicillin, 50 μ g/mL streptomycin (Gibco), and 16.6% fetal bovine serum (FBS; lot 192K18, Avantor). Cells were then plated onto tissue culture flasks (Corning). FACS was performed on single cells incubated with anti-mouse PDGFRA APC (clone APA5, eBioscience) to label FAPs, as previously described (13, 35). FACS-isolated FAPs were seeded at a density of 2000 cells/cm² onto tissue culture flasks (Corning) in growth media and maintained at 37°C in a humidified atmosphere with 5% CO₂. Media were changed every other day. Prior to use, FAPs were treated with 2 μ M (Z)-4-hydroxytamoxifen (Sigma-Aldrich) for 48 hours to induce inversion of the R206H-containing exon. All experiments were conducted with FAPs passaged fewer than 3 times.

Burn/tenotomy model of tHO. WT C57BL/6 mice were obtained from Taconic. The burn/tenotomy extremity-polytrauma model was performed as previously described (18, 19). Briefly, all mice received presurgical analgesia consisting of 0.06 mg/kg buprenorphine for 48 hours, followed by anesthesia with inhaled isoflurane, and close post-operative monitoring with analgesic administration. Mice received 30% total body surface area partial thickness burns on a shaved dorsum

followed by transection of the left Achilles tendon. Dorsal burn was induced using a metal block heated to 60°C in a water bath and continuously applied to the dorsum for 18 seconds. Heterotopic bone was quantified by μ CT 5 weeks after surgery.

Generation of type II receptor-knockout mES cells. mES cell lines ablated for *Acvr2a*, *Acvr2b*, and/or *Bmpr2* were generated as follows. Briefly, CRISPR guides targeting the 5' and 3' ends of the *Acvr2a* coding sequence were electroporated into an mES cell line harboring the tamoxifen inducible, conditional-on *Acvr1* R206H FOP allele (*Acvr1*^{[R206H]Flox/+}; *Gt(ROSA26)Sor*^{CreERT2/+}; ref. 8). mES cell clones with biallelic collapses for *Acvr2a* were identified by real-time qPCR analysis and then electroporated with CRISPR guides to biallelically ablate *Acvr2b*, generating the cell line *Acvr2a*^{-/-}; *Acvr2b*^{-/-}; *Acvr1*^{[R206H]Flox/+}; *Gt(ROSA26)Sor*^{CreERT2/+}. An *Acvr2a*^{-/-}; *Acvr2b*^{-/-}; *Bmpr2*^{-/-}; *Acvr1*^{[R206H]Flox/+}; *Gt(ROSA26)Sor*^{CreERT2/+} mES cell line was generated in a similar manner, as was a *Bmpr2*^{-/-}; *Acvr1*^{[R206H]Flox/+}; *Gt(ROSA26)Sor*^{CreERT2/+} mES cell line. All mES cell lines were then expanded for further experimentation.

Culturing mES cells and immunoblotting. mES cell lines were cultured on irradiated MEF puromycin-resistant feeders (Thermo Fisher Scientific, A34965) on gelatin-coated plates in complete KO-ES media (KO DMEM) (Gibco, 10829018) containing 15% (v/v) ES-screened FBS, 2 mM L-glutamine, 50 U/mL penicillin/streptomycin, 0.2% (v/v) β -mercaptoethanol, and 2 U/mL Leukemia Inhibitory Factor (Millipore, ESG1107) at 37°C in a humidified atmosphere with 5% CO₂. The feeder cells were removed using magnetic feeder removal microbeads (Miltenyi Biotec, 130-095-531) by following the manufacturer's protocol. Approximately 300,000 mES cells/well were plated in a 24-well gelatin-coated plate. After 24 hours of growing in 2i media (36), mES cells were treated with 100 nM tamoxifen in 2i media for 24 hours to induce inversion of FOP mutant ACVR1 (8). On the following day, mES cells were switched to serum-free media for 2 hours before 1 hour treatment with various ligands, mAbs or Fabs. Subsequently, cells were lysed in RIPA buffer (Thermo Fisher Scientific, 89900) containing 2 \times protease and phosphatase inhibitors (Thermo Fisher Scientific, 78441). Total protein concentration was determined by BCA kit (Thermo Fisher Scientific, 23227). Equal amounts of protein (10 μ g) were resolved under reducing conditions in 4%–12% Novex WedgeWell gels (Invitrogen) and transferred to PVDF membranes (Advansta). Membranes were blocked with Superblock (Thermo Fisher Scientific, 37536) for 3 hours at room temperature and incubated with primary antibodies from Cell Signaling Technology at a 1:1000 dilution (anti-p-Smad1/5/8 [clone 41D10]), or 1:5000 (anti- β -actin [clone 8H10D10]) overnight at 4°C, followed by incubation with horseradish peroxidase-conjugated secondary antibody at a 1:5000 dilution (catalog 7074) for 3 hours at room temperature. Western Bright ECL HRP substrate was used for detection (Advansta, K-12045-D20). A minimum of 2 independent biological replicates were performed for each experimental condition.

Cell lines. HEK293 and W20 cell lines were purchased from ATCC and their identity was confirmed by STR profiling. HEK293/BRE-luciferase stable cells were generated in-house using pGL4(luc2P/2XBRE/Puro) Smad1/5/8-responsive firefly luciferase vector (Promega, CS183203).

Immunoprecipitation. W20 cells and HEK293 cells were grown in DMEM containing 10% (v/v) FBS, 50 U/mL penicillin/streptomycin, and 2 mM L-glutamine. These cells were transfected with Myc-ACVR1, Myc-ACVR1[R206H], and HA-ACVRIIB alone or in various combinations. W20 cells were transfected using X-tremeGENE 9 DNA transfection reagent (Sigma-Aldrich, 06 365 787 001) and HEK293 cells were

transfected using TransIT-293 DNA transfection (MirusBio, MIR 2700) by following the manufacturers' protocols. After transfections, cells were incubated overnight in the complete media. The following day, cells were switched to serum-free media (in the presence or absence of ACVRIIB-Fc). Forty-eight hours after transfection, membrane fractions of the transfected cells were isolated using the Mem-PER Plus membrane protein extraction kit (Thermo Fisher Scientific, 89842). Membrane fractions were resuspended in the lysis buffer of the Myc-IP kit (Thermo Fisher Scientific, 88844) and Myc immunoprecipitation was performed using isolated membrane fractions by following the manufacturer's protocol. Immunoblotting was performed using immunoprecipitation input and elution samples as described above. Anti-ACVR1 antibody (Abcam, ab155981) and anti-HA antibody (Cell Signaling Technology, 3724) were used to detect Myc-ACVR1 and HA-ACVRIIB, respectively.

Reporter gene assay. HEK293/BRE-luciferase (Smad1/5/8-responsive) stable pools of reporter cells were generated. Reporter gene assay was performed as previously described (8). Briefly, approximately 10,000 cells/well were plated in a 96-well plate in complete media. After 16 hours of incubation with ligands alone or in the presence of anti-ACVR1 mAbs and Fabs, luciferase expression was measured using the Bright-Glo luciferase assay system (Promega, E2650).

DmrB homodimerization assay. HEK293/BRE-Luc stable cells were transfected with hACVR1-DmrB or hACVR1[R206H]-DmrB vector. High-ACVR1-expressing cells were isolated with FACS as previously described (8). Approximately 10,000 cells/well were plated in a 96-well plate in complete media. After 16 hours of incubation with B/B homodimerizer (Takara Bio, 635059) at various concentrations, luciferase expression was measured using the Bright-Glo luciferase assay system. In order to confirm the activity of the generated DmrB cell lines, HEK293.BRE.hACVR1-DmrB and HEK293.BRE.hACVR1[R206H]-DmrB cells were treated with 20 nM B/B homodimerizer for 16 hours in the serum-free media. The following day, these cells were treated with various concentrations of activin A or BMP7 in the 20 nM B/B homodimerizer-containing serum-free media. Sixteen hours after the ligand treatment, luciferase expression was measured using the Bright-Glo luciferase assay system.

Surface expression of ACVR1. *Acvr1*^{[R206H]/+} and *Acvr2a*^{-/-}; *Acvr2b*^{-/-}; *Bmpr2*^{-/-}; *Acvr1*^{[R206H]/+} mES cells were dissociated using nonenzymatic cell dissociation buffer (Millipore, S-004-B) and resuspended in flow cytometry staining buffer (R&D Systems, FC001). After 15 minutes of blocking (Thermo Fisher Scientific, 14-9161-73), cells were stained with anti-ACVR1 primary antibody (R&D Systems, MAB637) for 1 hour followed by staining with Alexa Fluor 647-conjugated secondary antibody (Thermo Fisher Scientific, A-21236) for 30 minutes. Stained cells were fixed with CytoFix (BD Biosciences, 554655) and passed through a filter block (Pall, PN 8027). All the steps were carried out in the flow cytometry staining buffer in the dark and on ice. Stained cells were analyzed using a CytoFLEX (Beckman) instrument.

Binding kinetics measurements. Kinetic binding parameters for the interaction of anti-ACVR1 mAbs and Fabs with human and mouse ACVR1 were determined on a Biacore T200 using dextran-coated (CM5) chips at 37°C. The running buffer was prepared using filtered HBS-EP (10 mM Hepes, 150 mM NaCl, 3.4 mM EDTA, 0.05% polysorbate 20, pH 7.4). In order to measure anti-ACVR1 mAb interactions with human and mouse ACVR1, an anti-hFc antibody was immobilized on a CM5 chip as previously described (9). After capturing approximately 250 response units (RU) of anti-ACVR1 mAbs, hACVR1.mmh and mACVR1.

mmh were injected over anti-ACVR1 mAbs at 50 $\mu\text{L}/\text{min}$ for 90 seconds followed by 20 minutes of dissociation. In order to measure anti-ACVR1 Fab interactions with human and mouse ACVR1, an anti-Myc antibody was immobilized on a CM5 chip. After capturing equal RUs of a mouse or human ACVR1.mmh on the surface, anti-ACVR1 Fabs were injected at 50 $\mu\text{L}/\text{min}$ for 90 seconds followed by 20 minutes of dissociation. Kinetic parameters were obtained by globally fitting the real-time binding data to a 1:1 Langmuir binding model using Scrubber 2.0c Evaluation software (<http://www.biologic.com.au/scrubber.html>). The equilibrium dissociation constant (K_D) was calculated by dividing the dissociation rate constant (k_d) by the association rate constant (k_a).

Statistics. Statistical analysis was performed using Prism 9 software (GraphPad) and results are represented as mean \pm SD unless otherwise indicated. Comparisons of 2 groups were evaluated using an unpaired 2-tailed Student's *t* test. Comparisons of more than 2 groups were evaluated using 1-way ANOVA followed by a multiple-comparison test (Dunnett's or Bonferroni's). For all tests, a *P* value of less than 0.05 was considered significant.

Study approval. All experiments were performed in accordance with the Institutional Animal Care and Use Committee of Regeneron.

Author contributions

SJH, VI, and ANE designed the study and analyzed data. SA, LH, LW, NMD, SR, YR, QZ, NR, KCN, VK, SB, LT, JLS, and KS carried out the experiments and analyzed data. SJH, VI, ANE, PB, Y,

AJM, SA, SF, and LJ wrote the manuscript, which was reviewed by all authors. SA and LH contributed equally to the manuscript; assignment of order of authorship was alphabetical and based on their last names.

Acknowledgments

The authors thank the following contributors for providing support: the VelociGene team for generating the ES cells and mice used in this study and the vivarium staff for animal husbandry; members of the departments of Therapeutic Proteins, Protein Expression Sciences, and Preclinical Manufacturing and Process Development for immunization and production of antibodies, stable cell lines, and large-scale production of proteins; members of the DNA Core and Molecular Profiling for plasmid production and RNA sequencing analysis; and Jen Symonds and Tyler Billipp (Adimab) for help with antibody discovery and optimization. PBY has received funding support from the National Institutes of Health/National Institute for Arthritis and Musculoskeletal and Skin Diseases (NIH/NIAMS grant AR057374).

Address correspondence to: Sarah J Hatsell or Vincent Idone or Aris N Economides, Regeneron Pharmaceuticals Inc, 777 Old Saw Mill River Road, Tarrytown, New York 10591, USA. Email: Sarah.hatsell@regeneron.com (SJH); Email: Vincent.idone@regeneron.com (VI); Email: aris@regeneron.com (ANE).

- Pignolo RJ, et al. Natural history of fibrodysplasia ossificans progressiva: cross-sectional analysis of annotated baseline phenotypes. *Orphanet J Rare Dis.* 2019;14(1):98.
- Shore EM, et al. A recurrent mutation in the BMP type I receptor ACVR1 causes inherited and sporadic fibrodysplasia ossificans progressiva. *Nat Genet.* 2006;38(5):525–527.
- Petrie KA, et al. Novel mutations in ACVR1 result in atypical features in two fibrodysplasia ossificans progressiva patients. *PLoS One.* 2009;4(3):e5005.
- Huning I, Gillesen-Kaesbach G. Fibrodysplasia ossificans progressiva: clinical course, genetic mutations and genotype-phenotype correlation. *Mol Syndromol.* 2014;5(5):201–211.
- Kaplan FS, et al. Fibrodysplasia ossificans progressiva: mechanisms and models of skeletal metamorphosis. *Dis Model Mech.* 2012;5(6):756–762.
- Gorter DJJ, et al. Promiscuous signaling of ligands via mutant ALK2 in fibrodysplasia ossificans progressiva. *Receptors Clin Invest.* 2016;3:397.
- Chakkalakal SA, et al. An Acvr1 R206H knock-in mouse has fibrodysplasia ossificans progressiva. *J Bone Miner Res.* 2012;27(8):1746–1756.
- Hatsell SJ, et al. ACVR1R206H receptor mutation causes fibrodysplasia ossificans progressiva by imparting responsiveness to activin A. *Sci Transl Med.* 2015;7(303):303ra137.
- Aykul S, et al. Activin A forms a non-signaling complex with ACVR1 and type II Activin/BMP receptors via its finger 2 tip loop. *Elife.* 2020;9:e5482.
- Upadhyay J, et al. The expansion of heterotopic bone in fibrodysplasia ossificans progressiva is activin A-dependent. *J Bone Miner Res.* 2017;32(12):2489–2499.
- Hino K, et al. Neofunction of ACVR1 in fibrodysplasia ossificans progressiva. *Proc Natl Acad Sci U S A.* 2015;112(50):15438–15443.
- Dey D, et al. Two tissue-resident progenitor lineages drive distinct phenotypes of heterotopic ossification. *Sci Transl Med.* 2016;8(366):366ra163.
- Lees-Shepard JB, et al. Activin-dependent signaling in fibro/adipogenic progenitors causes fibrodysplasia ossificans progressiva. *Nat Commun.* 2018;9(1):471.
- Lees-Shepard JB, et al. An anti-ACVR1 antibody exacerbates heterotopic ossification by fibro-adipogenic progenitors in fibrodysplasia ossificans progressiva mice. 2022;132(12):e153795.
- Rouha H, et al. Five birds, one stone: neutralization of α -hemolysin and 4 bi-component leukocidins of *Staphylococcus aureus* with a single human monoclonal antibody. *MAbs.* 2015;7(1):243–254.
- Korchynskiy O, ten Dijke P. Identification and functional characterization of distinct critically important bone morphogenetic protein-specific response elements in the Id1 promoter. *J Biol Chem.* 2002;277(7):4883–4891.
- Fujii M, et al. Roles of bone morphogenetic protein type I receptors and Smad proteins in osteoblast and chondroblast differentiation. *Mol Biol Cell.* 1999;10(11):3801–3813.
- Peterson JR, et al. Burn injury enhances bone formation in heterotopic ossification model. *Ann Surg.* 2014;259(5):993–998.
- Hwang C, et al. Activin A does not drive post-traumatic heterotopic ossification. *Bone.* 2020;138:115473.
- Steinbicker AU, et al. Perturbation of hepcidin expression by BMP type I receptor deletion induces iron overload in mice. *Blood.* 2011;118(15):4224–4230.
- Andriopoulos B Jr, et al. BMP6 is a key endogenous regulator of hepcidin expression and iron metabolism. *Nat Genet.* 2009;41(4):482–487.
- Meynard D, et al. Lack of the bone morphogenetic protein BMP6 induces massive iron overload. *Nat Genet.* 2009;41(4):478–481.
- Clackson T, et al. Redesigning an FKBP-ligand interface to generate chemical dimerizers with novel specificity. *Proc Natl Acad Sci U S A.* 1998;95(18):10437–10442.
- Kaplan FS, et al. Multi-system involvement in a severe variant of fibrodysplasia ossificans progressiva (ACVR1 c.772G>A; R258G): a report of two patients. *Am J Med Genet A.* 2015;167A(10):2265–2271.
- Le VQ, Wharton KA. Hyperactive BMP signaling induced by ALK2(R206H) requires type II receptor function in a *Drosophila* model for classic fibrodysplasia ossificans progressiva. *Dev Dyn.* 2012;241(1):200–214.
- Bagarova J, et al. Constitutively active ALK2 receptor mutants require type II receptor cooperation. *Mol Cell Biol.* 2013;33(12):2413–2424.
- Ramachandran A, et al. Pathogenic ACVR1(R206H) activation by Activin A-induced receptor clustering and autophosphorylation. *EMBO J.* 2021;40(14):e106317.
- Ehrlich M, et al. Homomeric and heteromeric complexes among TGF- β and BMP receptors and their roles in signaling. *Cell Signal.* 2011;23(9):1424–1432.

29. Katagiri T, et al. An antibody against ALK2 extracellular domain reveals a role of dimer formation for signal activation. *J Bone Miner Res.* 2018;33(s1):S1-S464.
30. Yaden BC, et al. Inhibition of activin A ameliorates skeletal muscle injury and rescues contractile properties by inducing efficient remodeling in female mice. *Am J Pathol.* 2014;184(4):1152-1166.
31. Fukuda T, et al. Generation of a mouse with conditionally activated signaling through the BMP receptor, ALK2. *Genesis.* 2006;44(4):159-167.
32. Xu Y, et al. Addressing polyspecificity of antibodies selected from an in vitro yeast presentation system: a FACS-based, high-throughput selection and analytical tool. *Protein Eng Des Sel.* 2013;26(10):663-670.
33. Economides AN, et al. Conditionals by inversion provide a universal method for the generation of conditional alleles. *Proc Natl Acad Sci U S A.* 2013;110(34):E3179-E3188.
34. Liu F, et al. Hydrodynamics-based transfection in animals by systemic administration of plasmid DNA. *Gene Ther.* 1999;6(7):1258-1266.
35. Lees-Shepard JB, et al. Palovarotene reduces heterotopic ossification in juvenile FOP mice but exhibits pronounced skeletal toxicity. *Elife.* 2018;7:e40814.
36. Tamm C, et al. A comparative study of protocols for mouse embryonic stem cell culturing. *PLoS One.* 2013;8(12):e81156.